Science of the Total Environment 814 (2022) 152575

Contents lists available at ScienceDirect

Science of the Total Environment

journal homepage: www.elsevier.com/locate/scitotenv

The underappreciated role of monocarbonyl-dicarbonyl interconversion in secondary organic aerosol formation during photochemical oxidation of m-xylene

Jiangyao Chen [a,b,*], Jiani Li [a], Xiaoyan Chen [a], Jianwei Gu [a,b], Taicheng An [a,b]

[a] Guangdong Key Laboratory of Environmental Catalysis and Health Risk Control, Guangdong Technology Research Center for Photocatalytic Technology Integration and Equipment Engineering, Institute of Environmental Health and Pollution Control, Guangdong University of Technology, Guangzhou 510006, China

[b] Guangzhou Key Laboratory of Environmental Catalysis and Pollution Control, Guangdong-Hong Kong-Macao Joint Laboratory for Contaminants Exposure and Health, School of Environmental Science and Engineering, Guangdong University of Technology, Guangzhou 510006, China

HIGHLIGHTS

- Main product switching from dicarbonyl to monocarbonyl during oxidation of m-xylene
- Photolysis of dicarbonyl converts to monocarbonyl, favoring SOA formation.
- Photopolymerization of monocarbonyl to dicarbonyl decreases SOA production.
- OH promotes production of both monocarbonyl and SOA from dicarbonyl.
- Mixed dicarbonyl inhibits their conversion to monocarbonyl and reduces SOA yield.

GRAPHICAL ABSTRACT

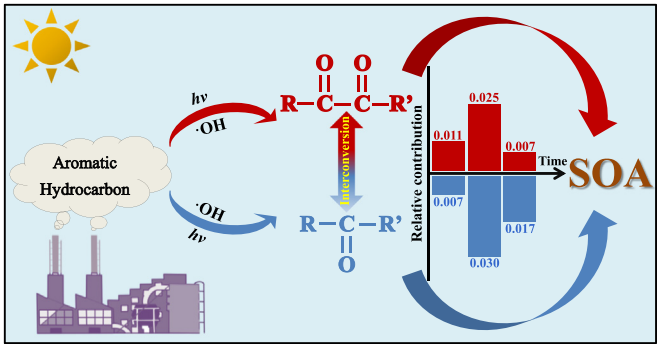

ARTICLE INFO

Article history:
Received 30 October 2021
Received in revised form 6 December 2021
Accepted 16 December 2021
Available online 25 December 2021

Editor: Pingqing Fu

Keywords:
Aromatic hydrocarbon
Photochemical oxidation
Carbonyl interconversion
Secondary organic aerosols
Atmospheric fate

ABSTRACT

Photochemical oxidation (including photolysis and OH-initiated reactions) of aromatic hydrocarbon produces carbonyls, which are involved in the formation of secondary organic aerosols (SOA). However, the mechanism of this process remains incompletely understood. Herein, the monocarbonyl-dicarbonyl interconversion and its role in SOA production were investigated via a series of photochemical oxidation experiments for m-xylene and representative carbonyls. The results showed that SOA mass concentration peaked at 113.5 ± 3.5 μg m^{-3} after m-xylene oxidation for 60 min and then decreased. Change in the main oxidation products from dicarbonyl (e.g., glyoxal, methylglyoxal) to monocarbonyl (e.g., formaldehyde) was responsible for this decrease. The photolysis of methylglyoxal or glyoxal produced formaldehyde, favoring SOA formation, while photopolymerization of formaldehyde to glyoxal decreased SOA production. The presence of ·OH altered the balance of photolysis interconversion, resulting in greater production of formaldehyde and SOA from glyoxal than methylglyoxal. Both photolysis and OH-initiated transformations of glyoxal to formaldehyde were suppressed by methylglyoxal, while glyoxal accelerated the reaction of ·OH with methylglyoxal to generate products which reversibly converted to glyoxal and methylglyoxal. These interconversion reactions reduced SOA production. The present study provides a new research perspective for the contribution mechanism of carbonyls in SOA formation and the findings are also helpful to efficiently evaluate the atmospheric fate of aromatic hydrocarbons.

* Corresponding author at: Guangzhou Key Laboratory of Environmental Catalysis and Pollution Control, Guangdong-Hong Kong-Macao Joint Laboratory for Contaminants Exposure and Health, School of Environmental Science and Engineering, Guangdong University of Technology, Guangzhou 510006, China.
E-mail address: chenjiangyao@gdut.edu.cn (J. Chen).

http://dx.doi.org/10.1016/j.scitotenv.2021.152575

1. Introduction

Aromatic hydrocarbons (AHs) constitute 20%–30% of atmospheric volatile organic compounds and their photochemical oxidation results in the formation of secondary organic aerosols (SOA) (Hallquist et al., 2009; Herckes et al., 2013; Li et al., 2020; Chen et al., 2020). It has been confirmed that AHs (e.g., toluene, xylenes) contribute significantly more to SOA formation than other hydrocarbons (e.g., isoprene, monoterpenes) by a recent field observation from urban cities of Pearl River Delta, China (Wang et al., 2013). Till today, researchers have also attempted to elucidate the mechanisms and implications in the formation of SOA from photochemical oxidation of AHs with the help of theoretical models, on-site monitoring as well as experimental studies (Arey et al., 2009; Huang et al., 2013; Paulot et al., 2009; Teng et al., 2017; Luo et al., 2021). All available data reveal that intermediates from photochemical oxidation of AHs play an important role in the formation of SOA, and even influence its yield and composition (Henze et al., 2008; Riva et al., 2015; Song et al., 2019; Ji et al., 2020). Thus, comprehensive understanding of the evolution of intermediates during photochemical oxidation of AHs is helpful for revealing the formation mechanism of SOA in real atmosphere environment.

Researchers have identified the presence of aldehyde group of carbonyl compounds in SOA collected from real atmospheric environment (Duarte et al., 2005; Santos and Duarte, 1998). According to the number of aldehyde groups, these carbonyl compounds are divided into monocarbonyl and dicarbonyl, respectively (Li et al., 2019). Recent experimental studies report significant contribution to SOA formation from dicarbonyl (Li et al., 2016; Birdsall and Elrod, 2011), due to its high yield (31.9% to 60.2%) from photochemical oxidation of AHs (Volkamer et al., 2001; Tuazon et al., 1986). Atmospheric observation further confirms that high concentration of dicarbonyl, such as glyoxal and methylglyoxal, leads to high production of SOA (Ying et al., 2015). However, a recent work highlights the indispensable role of monocarbonyl (e.g., formaldehyde) in SOA formation (Rodriguez et al., 2017). The authors proposed that the presence of formaldehyde increased the formation rates of imidazole product in reactions with ammonium sulfate and amines, enhancing the production of SOA to approximately 1.05 Tg of C/year. Although available studies indicate the important contribution of monocarbonyl and dicarbonyl to SOA formation, the mechanism involved during photochemical oxidation of AHs is still unclear.

In addition, some studies observed the photochemical conversion between dicarbonyl and monocarbonyl. For example, Tadic et al. (2006) and Chen and Zhu (2003) successively reported photodissociation of glyoxal to formaldehyde, while Clifford et al. proposed transformation of *o*-methylbenzaldehyde to o-phthalaldehyde under light irradiation (Clifford et al., 2011). Furthermore, OH-initiated reaction of glyoxal (Feierabend et al., 2008) or 2-pentanone (Atkinson et al., 2000) to produce formaldehyde was also confirmed. Earlier studies have also suggested that the reactions of methylglyoxal with acetaldehyde and formaldehyde to form acetal (Li et al., 2011) or imidazole products (Kua et al., 2011; Sedehi et al., 2013), likely contribute to aqueous formation of SOA. These complex transformation reactions often result in more complicated roles of dicarbonyl and monocarbonyl in SOA formation, leading to misunderstanding of the corresponding contribution mechanism. Therefore, complete revelation of the conversion process between dicarbonyl and monocarbonyl is necessary to clarify the accurate contribution mechanism of carbonyl products in SOA formation during photochemical oxidation of AHs.

This study attempted to gain a deeper understanding of monocarbonyl-dicarbonyl interconversion and its role in SOA formation during photochemical oxidation of a typical AH, m-xylene. First, the monocarbonyl and dicarbonyl products were sampled, identified and quantified based on a combined method of derivatization, solid-phase microextraction (SPME) and gas chromatography–mass spectrometry (GC–MS). Then, their contributions to SOA formation were preliminarily investigated according to experiments with or without addition of representative monocarbonyl and dicarbonyl into original reaction. Furthermore, variations of carbonyl products as well as SOA formation under photolysis and photochemical oxidation of typical dicarbonyl were explored to establish the relationship between interconversion of carbonyl and SOA production. Finally, the experimental data of SOA yield were also compared with the data from classical theoretical model to further highlight the underappreciated role of mutual transformation between monocarbonyl and dicarbonyl in SOA formation.

2. Experimental

2.1. Photochemical oxidation experiments

All experiments were conducted in a custom-made steel reactor. The inside of the reactor was fixed with a 10 L pillow-shaped Teflon bag and eight black lamps (5 W, 365 nm). The bag was thoroughly flushed with high-purity nitrogen before and after each experiment to ensure negligible background value of carbonyls and SOA (Fig. S1a and S1b). In a typical experiment, 3 μL H_2O_2 (30%, Aladdin) and 0.1 μL m-xylene (99%, Aladdin) were successively injected into the bag. After mixing for 1 min, lamps were turned on to trigger the photochemical oxidation reaction. At given intervals, the gaseous sample was taken out for analysis. Similarly, experiments for photochemical oxidation of m-xylene with formaldehyde or glyoxal as well as photolysis and photochemical oxidation of glyoxal, methylglyoxal and their mixture were also conducted. The temperature and relative humidity (RH) in the Teflon bag were monitored and showed small fluctuation during reaction period (Fig. S1c and S1d). All experiments were repeated at least twice.

2.2. Analysis of m-xylene and its carbonyl products

Both m-xylene and its carbonyl products were analyzed by GC–MS (Agilent 7890B5977B) with the help of SPME (65 μm PDMS/DVB, Supelco). The residual m-xylene was directly sampled via SPME fiber and injected into GC–MS for concentration analysis. For carbonyl intermediates, O-(2,3,4,5,6-pentafluorobenzyl) hydroxylamine hydrochloride (PFBHA, CNW) was used as the derivatization reagent (Yu et al., 1995; Koziel et al., 2001; Pang et al., 2014). Typically, 1 mL PFBHA solution (0.4 mg mL^{-1}) was added into a headspace bottle and SPME fiber was then inserted to adsorb PFBHA vapor for 1 min. The PFBHA adsorbed fiber was subsequently placed into the Teflon bag at designed reaction intervals. Finally, the sampled fiber was taken out and quickly inserted into the injection port of GC. The temperature program of GC with an SH-Rxi-5Sil capillary column (30 m × 0.25 mm × 0.25 μm) was operated under the following conditions: initially 60 °C for 1 min, and elevated to 280 °C at a rate of 7 °C min^{-1} and held for 1 min. The MS full scan mode was carried out with *m/z* of 30–500, and the temperature of transfer line and ionizing energy were set to be 280 °C and 70 eV, respectively. The carrier gas was ultra-high purity helium with flow rate of 1.2 mL min^{-1}.

Qualitative and quantitative analysis of carbonyl products were accomplished with the help of the National Institute of Standards and Technology (NIST) database and commercial standard samples. In brief, specific amounts of commercial compounds were dissolved in methanol, injected into the Teflon bag for evaporation, sampled with derivatized SPME fiber and analyzed by GC–MS. Detailed concentrations of commercial carbonyls are given in Supporting Information.

2.3. Secondary organic aerosol measurement

The measurement of SOA was conducted by a scanning mobility particle sizer spectrometer (SMPS, 3938NL76, TSI), including aerosol size distribution, number and mass concentration, which was obtained from aerosol volume concentration by assuming a density of 1.4 g cm^{-3} for the condensed organic matter according to the reported references (Ng et al., 2007; Sato et al., 2010). Shell velocity and aerosol flow rate of SMPS were set as 3 and 0.3 L min^{-1}, and particle size ranged from 13.8 to 723.4 nm.

3. Results and discussion

3.1. SOA formation from photochemical oxidation of m-xylene

Photochemical oxidation of m-xylene for 45 min decreased its concentration from 2000 to 1679 ppb, consuming about 16.1% (Fig. S2a). At this moment, 2.74 ± 0.15 × 10^4 particles cm^{-3} of SOA was produced (Fig. 1a). At 60 and 120 min, 24.1% and 40.3% of m-xylene were oxidized, and the SOA number concentration increased to 3.51 ± 0.02 × 10^4 and 7.00 ± 0.27 × 10^4 particles cm^{-3}, respectively. Continuous consumption of m-xylene promoted the production of SOA. However, SOA mass concentration first increased from 25.7 ± 2.2 μg m^{-3} at 45 min to 113.5 ± 3.5 μg m^{-3} at 60 min and then decreased to 86.0 ± 1.3 μg m^{-3} at 120 min. Continuous increase in SOA mass concentration along with reaction time is typically observed during photochemical oxidation of volatile organics (Zhang et al., 2011; Zhang et al., 2019a). However, Song et al. recently observed that SOA mass concentration increased to peak value (50.0 μg m^{-3}) at 60 min and then rapidly decreased to zero at 240 min during oxidation of isoprene (Song et al., 2019). This trend was similar to the present work. The authors claimed that the decrease in SOA mass concentration was mainly ascribed to wall loss rather than shrinking of aerosol size distribution, since isoprene was almost completely consumed at 60 min. Conversely, Kroll et al. stated that the decrease in SOA mass concentration after its peak value was mainly due to the shrinking effect (Kroll et al., 2006).

In order to verify whether the shrinking effect was responsible for the decreased SOA mass concentration in this study, the percentage of SOA number at different size ranges was compared. As shown in Fig. S2b, the size of SOA displayed a wide range from 14.1 to 151.2 nm, which was accordingly divided into three segments (14.1–30.0, 31.1–63.8 and 66.1–151.2 nm) (Fig. S2c). At 45 min, the percentages of SOA number in the above three segments were 82.1%, 17.3% and 0.6%, suggesting that SOA with the smallest size was dominant. These percentages changed to 69.5%, 22.4% and 8.1% at 60 min. The enhanced percentage of SOA with larger size range revealed agglomeration of smaller particles, which was responsible for higher SOA mass concentration. However, about 93.8% of smallest sized SOA was obtained at 120 min, far higher than that in the other two size segments (5.1% and 1.1%), leading to much lower SOA mass concentration at this time. Clearly, shrinking of SOA size distribution contributed to the decrease in SOA mass concentration during photochemical oxidation of m-xylene.

Furthermore, different from the results from Song et al., about 76% and 60% of residual m-xylene were observed at 60 and 120 min in this work. Oxidation of m-xylene during this interval still produced intermediates, which were then converted to new SOA with small size. Hence, the synergetic effect of new small-sized SOA formation, aerosol size distribution shrinking as well as wall loss led to the decrease in SOA mass concentration in this study. Notably, some researchers indicated more significant correlation between change in mass concentration of SOA and variation of products (Perri et al., 2009). For instance, isoprene epoxydiols (IEPOX) are the oxidation products of isoprene, which were found to be positively correlated with average IEPOX-SOA (Hu et al., 2015). Compared with aerosol size distribution shrinking and wall loss, the contribution mechanism of oxidation product to SOA production is still unclear. Therefore, further analysis of the distribution of products is needed to obtain deeper knowledge regarding the decreased formation of SOA from photochemical oxidation of m-xylene.

3.2. Carbonyl products from photochemical oxidation of m-xylene

Carbonyls are recognized as the main contributors for SOA formation during photochemical oxidation of AHs. Here, carbonyl products were accordingly sampled by PFBHA-adsorbed SPME fiber at 5, 20, 45, 60 and 120 min, and detected by GC–MS (Figs. S3-S10). All mass spectra showed characteristic fragment ion at m/z = 181, which represented oxime product from reaction of carbonyl with PFBHA. This ion is typically used to identify carbonyls (Koziel et al., 2001; Pang et al., 2014). Standard compounds were also applied to identify and quantify carbonyl products (Figs. S4, S6, S8 and S10-S14).

As shown in Figs. 1b and S15, only formaldehyde, acetaldehyde and methylglyoxal were produced at 5 min, with concentrations of 9.5 ± 1.3, 3.3 ± 3.1 and 38.9 ± 0.4 ppb. Methylglyoxal accounted for 75.2% of total products, indicating its dominant formation from m-xylene at initial stage of reaction. However, the percentage of methylglyoxal sharply decreased to 15.1% at 45 min, although its concentration more than doubled (84.2 ± 6.9 ppb). This was due to significant formation of other carbonyls, including glyoxal (259.2 ± 18.0 ppb), methylcyclopentanone (29.5 ± 8.3 ppb), butyraldehyde (8.1 ± 1.1 ppb), m-tolualdehyde (7.4 ± 6.1 ppb), heptanal (3.9 ± 1.1 ppb), and pentanal (2.2 ± 0.6 ppb). At this moment, both concentration and percentage (46.6%) of glyoxal greatly exceeded those of methylglyoxal and other products such as formaldehyde (129.8 ± 16.1 ppb and 23.3%), suggesting that glyoxal was the main intermediate at 45 min. After reaction for another 15 min, the concentrations and percentages of glyoxal and methylglyoxal decreased to 153.4 ± 18.7 ppb and 33.2%, and 53.2 ± 15.9 ppb and 11.5%, while that of formaldehyde increased to 134.7 ± 12.6 ppb and 29.2%. Clearly, both concentration and percentage of glyoxal were still the most dominant among all products. However, at 120 min, no glyoxal was detected, while the concentration and percentage of methylglyoxal increased to 69.2 ± 19.1 ppb and 29.9%. Although its concentration decreased by 42.9 ppb, the percentage of formaldehyde was 1.4 times of that at 60 min.

Methylglyoxal, glyoxal and formaldehyde were the three main products formed during photochemical oxidation of m-xylene. Among them, the production of methylglyoxal was predominant at 5 min, and followed by formaldehyde. At 45 and 60 min, there was much higher production of glyoxal than formaldehyde and methylglyoxal. However, the production of formaldehyde became the highest at 120 min, and followed by methylglyoxal. The concentrations of these three main products changed significantly along with reaction time, due to their different formation pathways.

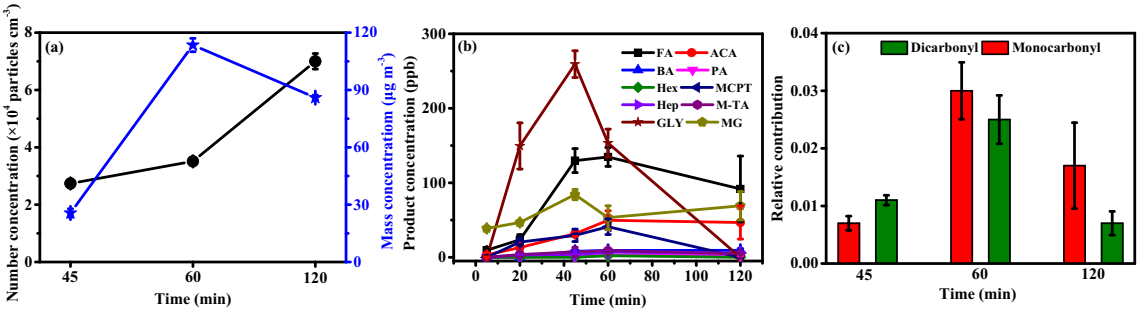

Fig. 1. SOA number and mass concentration (a), concentration of carbonyl product (b) and relative contribution of monocarbonyl and dicarbonyl (c) during photochemical oxidation of m-xylene. (FA: formaldehyde, ACA: acetaldehyde, BA: butyraldehyde, PA: pentanal, Hex: hexanal, Hep: heptanal, MCPT: methylcyclopentanone, M-TA: m-tolualdehyde, GLY: glyoxal, MG: methylglyoxal).

OH-initiated reaction of m-xylene consists of two pathways, H-abstraction from methyl group (about 4%) and OH-addition to aromatic ring (about 96%). The latter typically includes four pathways to produce ipso (MI), meta (MM) and two ortho (MOA and MOB) isomers, with branching ratios of 0.01, 0.02, 0.60 and 0.37, respectively (Fan and Zhang, 2008). Methylglyoxal is mostly generated from MOA pathway, while MOB pathway mainly produces glyoxal with methylglyoxal as minor product (Pan and Wang, 2014). Since MOA pathway accounts for a larger proportion of OH-addition reaction, the production of methylglyoxal is theoretically higher than that of glyoxal. Experimental results have also supported this conclusion (Arey et al., 2009; Gomez Alvarez et al., 2007; Nishino et al., 2010; Smith et al., 1999). In comparison with dicarbonyl, there are fewer studies focusing on the formation of monocarbonyl. Moreover, the pathway and ratio for generation of formaldehyde during OH-initiated reaction with AHs are still unclear. Recently, Li et al. reported that 42.3% of formaldehyde originated from methyl carbon of m-xylene (Li et al., 2017). This result indicated that the generation of formaldehyde is related to breakage of methyl group of m-xylene, and this pathway is totally different from that involved in the formation of glyoxal and methylglyoxal. Further investigations are necessary to better reveal the formation pathways of monocarbonyl and the potential relationship with dicarbonyl.

3.3. Contribution of monocarbonyl and dicarbonyl to SOA formation

According to the number of aldehyde groups, the ten carbonyl products were divided into two groups, monocarbonyl (e.g., formaldehyde, acetaldehyde, butyraldehyde, pentanal, hexanal, heptanal, 3-methylcyclopentanone and m-tolualdehyde) and dicarbonyl (e.g., glyoxal and methylglyoxal), to compare their contributions to SOA formation. Recently, Zhang et al. proposed an equation to evaluate the relative contribution (RC) of organics to SOA formation (Zhang et al., 2019b).

$$\mathrm{RC} = \frac{\Delta M_0}{\Delta HC} \times \frac{I_i}{\sum I_i} \quad (1)$$

where $\triangle M_0$ and $\triangle HC$ are SOA mass concentration and mass of reacted m-xylene. I_i and ΣI_i are peak intensity of *i-th* SOA component and sum of the peak intensities. As shown in Fig. 1c, the RC values of monocarbonyl and dicarbonyl were 0.007 ± 0.001 and 0.011 ± 0.001 at 45 min. Higher contribution of dicarbonyl to SOA generation was observed at this time. However, the RC of dicarbonyl (0.030 ± 0.005) was lower than that of monocarbonyl (0.025 ± 0.004) at 60 min, suggesting that the latter started contributing more to SOA formation. At 120 min, the RC of monocarbonyl (0.017 ± 0.007) was 2.4 times that of dicarbonyl (0.007 ± 0.002).

The change in main oxidation product from dicarbonyl to monocarbonyl contributed to the decreased SOA mass concentration. Elevated concentration of dicarbonyl and its RC for SOA were obtained before 60 min. Previous works also confirmed higher SOA yield from higher concentration of dicarbonyl (Arey et al., 2009; Yu et al., 1995; Fu et al., 2008; Ji et al., 2017), agreeing with the present result. After 60 min, although the concentration of monocarbonyl decreased, it became the dominant contributor in SOA formation (Fig. S16). In comparison with dicarbonyl, the contribution of monocarbonyl has been generally ignored in SOA production (Li et al., 2017; Edney et al., 2005; Marais et al., 2016), although a recent research reported that monocarbonyl accelerated the aqueous-phase generation of imidazoles and thus was involved in SOA formation (Rodriguez et al., 2017). The current results indicated that there existed an intrinsic relationship between monocarbonyl and dicarbonyl during photochemical oxidation of m-xylene, switching their contribution to SOA formation.

To verify the above deduction, 140 ppb glyoxal was added into the photochemical oxidation reaction of m-xylene at 45 min. The concentration of glyoxal quickly increased to 341.8 ± 23.1 ppb (Fig. 2a), while that of formaldehyde showed slight fluctuation (130.1 ± 14.5 ppb). After reaction for 15 min, the residual concentration of glyoxal was 200.1 ± 14.2 ppb, about 1.3 times of that in the original reaction (Fig. 2b). Higher consumption of glyoxal (35.9 ppb) was observed in this reaction, suggesting favorable oxidation of glyoxal with higher initial concentration. During this period, the concentration of formaldehyde decreased to 125.3 ± 7.8 ppb, while that in the original reaction increased to 134.7 ± 12.6 ppb. Addition of glyoxal into the photochemical oxidation of m-xylene was not conducive to formaldehyde production. Hence, the extra consumption of glyoxal was directed to SOA formation, since the SOA mass concentration was increased to 4.7 μg m^{-3} after glyoxal addition (Fig. 2e).

After adding 140 ppb formaldehyde instead of glyoxal into the original reaction, the instantaneous concentrations of formaldehyde and glyoxal in the system were 270.4 ± 4.9 and 455.7 ± 36.0 ppb (Fig. 2c). The concentration of glyoxal was increased to 75.8%, indicating significantly accelerated accumulation of glyoxal after formaldehyde injection. It is known that ·OH preferentially reacts with m-xylene instead of glyoxal to generate formaldehyde, due to the higher rate constant (2.36 × 10^{-11} cm^3 $molecule^{-1}$ s^{-1} for m-xylene and 1.14 × 10^{-11} cm^3 $molecule^{-1}$ s^{-1} for glyoxal) (Atkinson, 1986). Enhanced concentration of formaldehyde slowed the reaction between glyoxal and ·OH, leading to accumulation of glyoxal. Prolonging the reaction time to 60 min decreased the concentration of glyoxal to 341.4 ± 58.8 ppb (Fig. 2d), which was 120% higher than that in the original reaction. At this time, the SOA mass concentration was 23.8 ± 15.5 μg m^{-3} (Fig. 2e), only one fifth of that in original reaction, revealing remarkably suppressed SOA formation. This was due to reduced consumption of glyoxal after formaldehyde injection.

More experiments were performed to better understand the contributions of glyoxal and formaldehyde to SOA formation. Photochemical oxidation of 70, 140, 210 or 288 ppb glyoxal with 0.1 μL H_2O_2 for 20 min produced 5.2 ± 5.0, 5.5 ± 2.5, 9.5 ± 5.0 or 12.3 ± 6.7 μg m^{-3} of SOA (Fig. 3a). SOA mass concentration was positively correlated with initial concentration of glyoxal. Similar phenomenon was also observed for formaldehyde. About 2.2 ± 0.4 and 5.0 ± 0.3 μg m^{-3} of SOA were obtained from oxidation of 140 and 210 ppb formaldehyde, respectively. Under the same initial concentration, the SOA production from glyoxal was more than 1.9 times of that from formaldehyde, verifying the higher contribution of the former to SOA formation than the latter. In addition, photochemical oxidation of a mixture of glyoxal (288 ppb) and formaldehyde (140 ppb) produced 7.3 ± 1.2 μg m^{-3} of SOA, only 59.3% of that from neat glyoxal (288 ppb). The photochemical oxidation of glyoxal to form SOA was obviously inhibited in the presence of formaldehyde.

The concentration variation of formaldehyde and glyoxal during the above reactions was also monitored based on analysis of GC–MS information (Figs. S17-S19). Photochemical oxidation of 70 to 288 ppb glyoxal for 20 min consumed 31.4 ± 8.3 to 70.1 ± 15.8 ppb, accompanied by the formation of 17.6 ± 8.3 to 46.7 ± 18.5 ppb formaldehyde (Fig. 3b and c). Increasing the initial concentration of glyoxal favored its conversion to formaldehyde. Previous study claimed that formation of formaldehyde was one of the most important OH-initiated reactions for glyoxal (Feierabend et al., 2008), supporting the present conclusion. Together with SOA results, it was concluded that the transformation of glyoxal to formaldehyde promoted SOA production. In addition, 38.2 ± 16.2 ppb of glyoxal was consumed to produce 24.5 ± 9.4 ppb of formaldehyde after photochemical oxidation of their mixture for 20 min. The above altered concentrations were approximately half of that from photochemical oxidation of single glyoxal (288 ppb). Thus, the presence of formaldehyde inhibited the photochemical oxidation of glyoxal, decreasing the formation of SOA.

To sum up, during photochemical oxidation of m-xylene, the conversion of glyoxal to formaldehyde occurred, which was responsible for the transition of the dominant products from dicarbonyl to monocarbonyl. This transition further led to decline in SOA formation. Significantly, the increased concentration of glyoxal after formaldehyde addition was due to other formation mechanisms rather than extra production from oxidation of m-xylene, suggesting the existence of a reversible transformation between these two carbonyls.

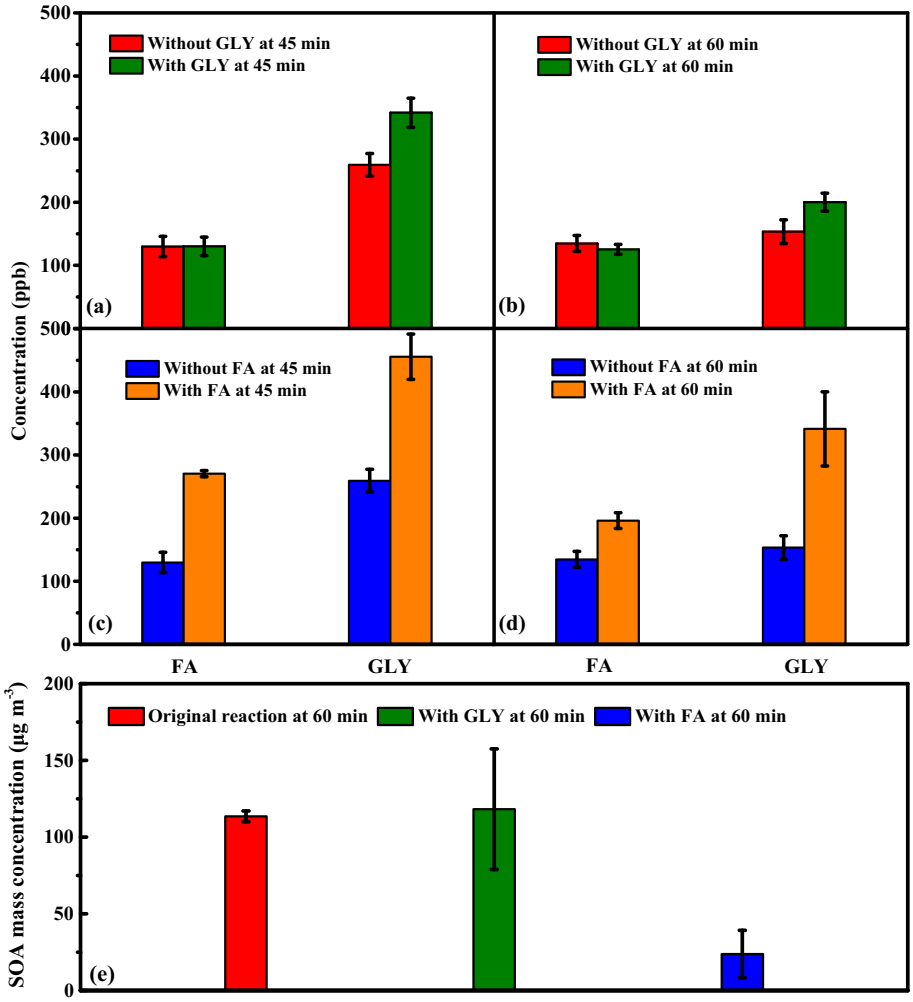

Fig. 2. Concentration of formaldehyde, glyoxal and SOA mass from photochemical oxidation of m-xylene with and without addition of glyoxal (a, b, e) and formaldehyde (c, d, e). (FA: formaldehyde, GLY: glyoxal).

3.4. Role of monocarbonyl-dicarbonyl interconversion in SOA formation

In general, photochemical oxidation includes direct photolysis and OH-initiated reactions, each of which might show different effects on the conversion between dicarbonyl and monocarbonyl. Here, by adding 0.1 μL H_2O_2, the photolysis and photochemical oxidation of single or mixed dicarbonyl (e.g., glyoxal, methylglyoxal with initial concentration of 2000 ppb) to monocarbonyl (e.g., formaldehyde) as well as their potential reversible transformation were investigated. Figs. S20-S25 display the corresponding total ion chromatograms and standard curves.

About 1710.8 ± 51.1 ppb glyoxal remained after its photolysis for 10 min, producing 201.2 ± 13.6 ppb formaldehyde (Fig. 4a and b). By extending the reaction time to 20 and 30 min, the concentration of glyoxal increased to 1725.6 ± 63.9 and 1848.7 ± 12.0 ppb, while that of formaldehyde decreased to 193.8 ± 14.4 and 105.2 ± 8.7 ppb. The concentrations of glyoxal and formaldehyde were 1837.9 ± 26.2 and 116.7 ± 11.3 ppb at 60 min. At the beginning of photolysis reaction, rapid decomposition of glyoxal to formaldehyde occurred. Then, formaldehyde conversely polymerized to glyoxal. Finally, the processes of decomposition and polymerization reached equilibrium. Evidently, there was interconversion between glyoxal and formaldehyde under light irradiation. Hepburn et al. reported that the major photolysis dissociation product of glyoxal was formaldehyde (Hepburn et al., 1983) while Clifford et al. observed that the main product during photolysis of *o*-methylbenzaldehyde was o-phthalaldehyde (Clifford et al., 2011), partially supporting the present results.

Photochemical oxidation of glyoxal for 10 min resulted in its decreased concentration (1667.2 ± 286.9 ppb), producing 232.2 ± 9.1 ppb formaldehyde. The consumption of glyoxal and production of formaldehyde in the photochemical oxidation system were 20% higher than that in the photolysis system, confirming the enhanced conversion of glyoxal to formaldehyde by ·OH. When the reaction time was prolonged to 60 min, the concentration of glyoxal continuously decreased to 1132.3 ± 88.7 ppb and the concentration of formaldehyde increased to 371.3 ± 8.6 ppb. In photochemical oxidation system, the balance of photolysis decomposition and polymerization between glyoxal and formaldehyde was broken by ·OH, accelerating the transformation of glyoxal to formaldehyde.

Different conversion mechanisms between dicarbonyl and monocarbonyl under light irradiation and ·OH attack were responsible for their different evolution pathways in the two systems. Chen et al. reported that the photolysis of glyoxal involved the initial formation of HCO radical and then formaldehyde (Chen and Zhu, 2003). Clifford et al. proposed that the photolysis transformation of *o*-methylbenzaldehyde to o-phthalaldehyde underwent an initial $n \rightarrow \pi^*$ electron conversion via photoexcitation of CO group, followed by H atom extraction from OH group and finally O_2 addition on methyl group of side chain (Clifford et al., 2011). Atkinson et al. found that the reaction pathways of ·OH with two carbonyls, 2-pentanone and 2-heptanone, both first involved H atom extraction from methyl group and then reactions with oxygen, isomerization and decomposition to preferentially generate formaldehyde (Atkinson et al., 2000). Further hydrogen abstraction reaction of formaldehyde by ·OH to form H_2O was theoretically and experimentally confirmed (Alvarez-Idaboy et al., 2001; Butkovskaya and Setser, 1998). Moreover, the

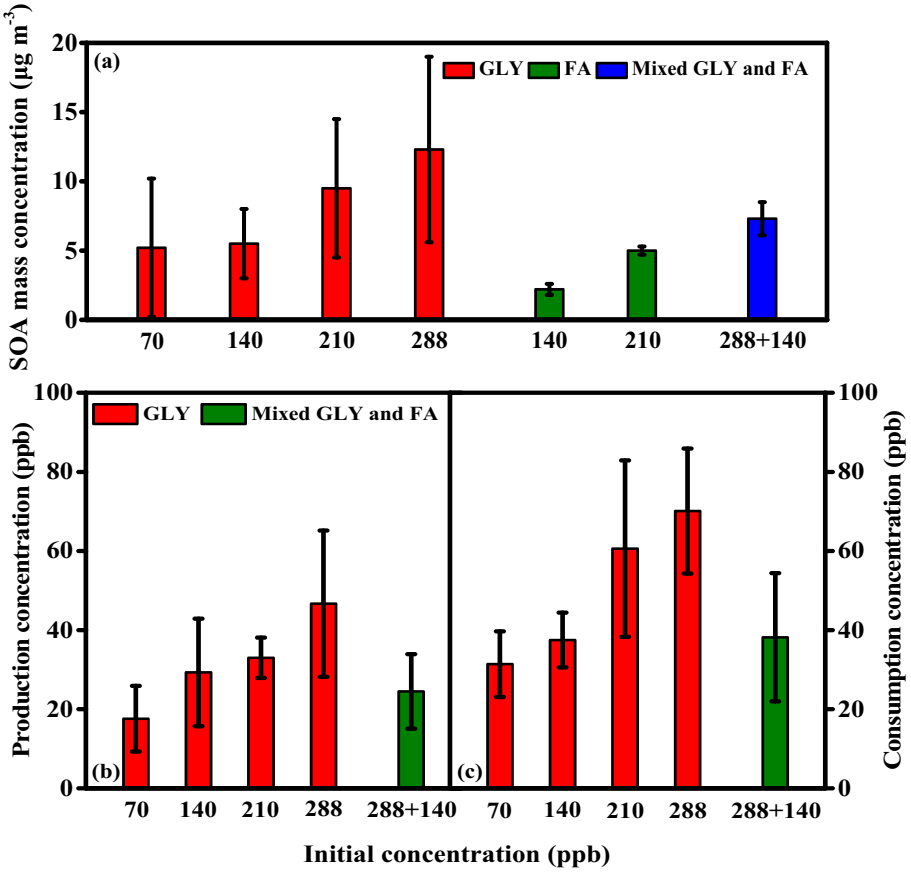

Fig. 3. SOA mass concentration (a), formaldehyde production (b) and glyoxal consumption (c) from photochemical oxidation of single or mixed glyoxal and formaldehyde. (FA: formaldehyde, GLY: glyoxal).

lifetime of glyoxal photodissociation was appreciably shorter than that of its reaction with ·OH, while glyoxal (1.14×10^{-11} cm^3 $molecule^{-1}$ s^{-1}) and formaldehyde (1.05×10^{-11} cm^3 $molecule^{-1}$ s^{-1}) showed similar reaction rate constants with ·OH (Plum et al., 1983; Stief et al., 1980).

Therefore, in the initial stage of photolysis reaction, glyoxal quickly dissociated to HCO radical, which was then converted to formaldehyde. Then, the photon attacked CO group of formaldehyde to trigger polymerization reaction and generate glyoxal. The above interconversion reactions led to opposite variation trend of concentration for glyoxal and formaldehyde in photolysis system. However, the reversible reactions of photodissociation and photopolymerization were affected in photochemical oxidation system, where ·OH simultaneously extracted H atom from CH group of glyoxal and formaldehyde to separately produce formaldehyde and H_2O, promoting the conversion of glyoxal to formaldehyde. The promoted transformation of glyoxal to formaldehyde also led to enhanced production of SOA. Within 60 min, the SOA mass concentrations from photolysis and photochemical oxidation of glyoxal were in the ranges of 0.8 ± 0.1 to 11.5 ± 4.7 μg m^{-3} and 1.5 ± 0.6 to 84.0 ± 21.9 μg m^{-3}, respectively (Fig. 4d). In the presence of ·OH, the SOA production nearly doubled at the beginning of the reaction and increased by a factor of seven at the end of the reaction. Hence, the promoted conversion of glyoxal to formaldehyde by ·OH suitably explains the observation of low SOA production under high formaldehyde concentration in Section 3.3.

Photolysis and photochemical oxidation of methylglyoxal were also conducted. About 1767.4 ± 116.3 ppb methylglyoxal remained after photolysis for 10 min (Fig. 4c), accompanied by the production of 55.8 ± 13.1 ppb formaldehyde (Fig. 4b). At 20 min, the concentration of formaldehyde was unchanged (55.7 ± 8.8 ppb), while that of methylglyoxal further decreased to 1495.7 ± 406.8 ppb, suggesting photolysis of methylglyoxal into other products than formaldehyde. After reaction for another 10 min, about 10.6 ± 9.0 ppb glyoxal was newly generated (Fig. 4a), while the concentration of methylglyoxal increased to 1524.4 ± 219.5 ppb and the concentration of formaldehyde decreased to 39.4 ± 4.7 ppb. When the reaction lasted for 60 min, the concentrations of methylglyoxal and glyoxal significantly increased to 1863.2 ± 154.0 and 199.3 ± 21.5 ppb, while that of formaldehyde showed little fluctuation (41.2 ± 4.9 ppb). Formaldehyde was a direct photolysis product of methylglyoxal, while glyoxal was converted from formaldehyde and other photolysis products of methylglyoxal. Regardless, both formaldehyde and glyoxal were formed as products during photolysis of methylglyoxal. Chen et al. reported the initial photolysis of methylglyoxal to HCO and COCHO radicals, which were then converted to formaldehyde and glyoxal (Chen et al., 2000), supporting the present results. Notably, the obviously increased concentrations of methylglyoxal and glyoxal from 30 to 60 min were mainly due to transformations from other photolysis products of methylglyoxal in addition to formaldehyde.

In photochemical oxidation system, 471.4 ppb of methylglyoxal was consumed within 10 min, twice of that from photolysis reaction. At this moment, both 139.6 ± 95.5 ppb glyoxal and 65.5 ± 0.9 ppb formaldehyde were detected. Oxidation of methylglyoxal by ·OH preferentially produced glyoxal. As the reaction time was prolonged, the concentration of methylglyoxal first decreased to 1265.7 ± 238.6 ppb at 20 min and then increased to 1473.5 ± 80.4 at 60 min. Methylglyoxal concentration showed the identical trend of initial decrease and then increase in both photolysis and photochemical oxidation systems, again indicating the occurrence of interconversion between methylglyoxal and its products. Moreover, inverted V-shaped and V-shaped concentration variations were observed for glyoxal and formaldehyde, respectively. Together with photolysis results, it was confirmed that mutual transformations occurred among methylglyoxal, glyoxal, formaldehyde and undetected products of methylglyoxal during photochemical oxidation of methylglyoxal.

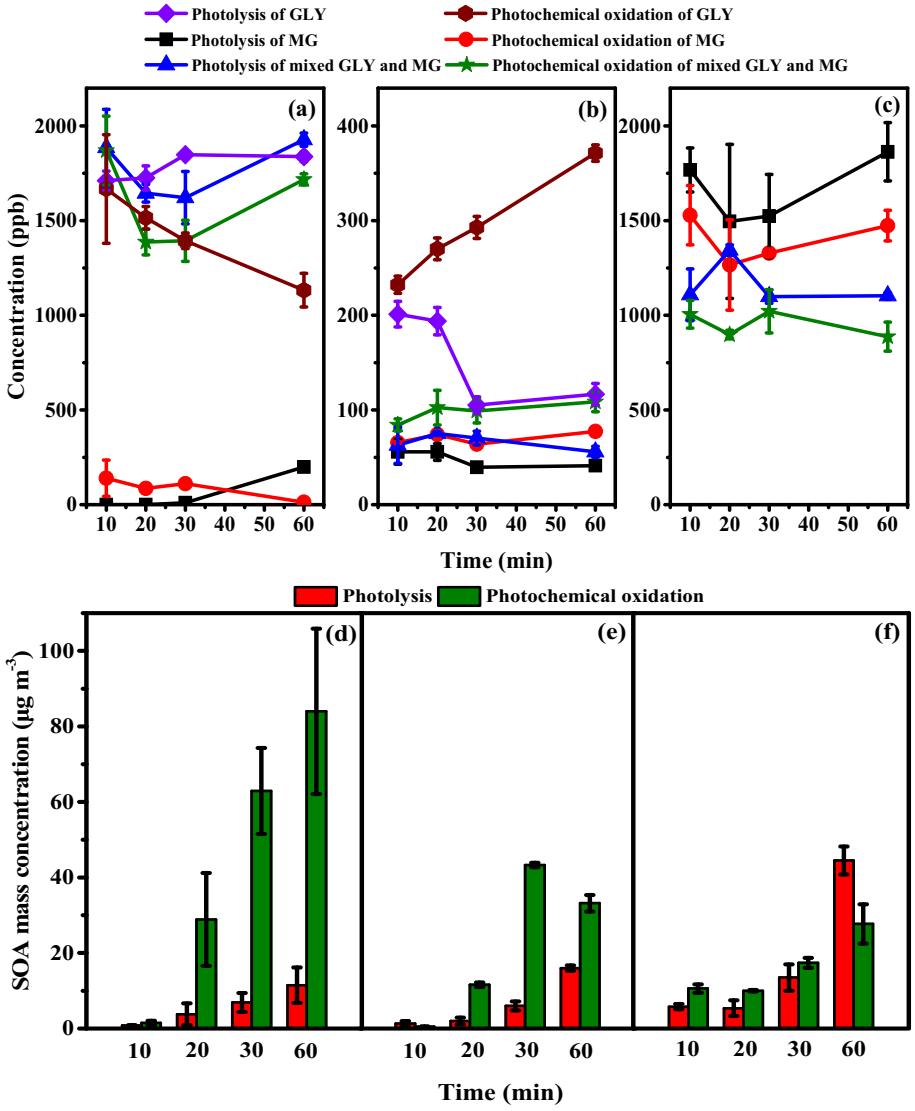

Fig. 4. Concentration of glyoxal (a), formaldehyde (b) and methylglyoxal (c), and SOA mass (d-e) during photolysis and photochemical oxidation of single glyoxal, methylglyoxal and mixture of them. (FA: formaldehyde, GLY: glyoxal, MG: methylglyoxal).

The mass concentration of SOA gradually increased from 1.3 ± 0.7 μg m^{-3} at 10 min to 16.0 ± 0.7 μg m^{-3} at 60 min during photolysis of methylglyoxal (Fig. 4e). These values were comparable to those from glyoxal photolysis, indicating identical contributions of these two dicarbonyl compounds to SOA formation under light irradiation. Photochemical oxidation of methylglyoxal doubled the SOA mass concentration to 33.2 ± 2.2 μg m^{-3} at 60 min compared to photolysis reaction. Similar to glyoxal, reaction of methylglyoxal with ·OH obviously increased the SOA production. However, a greater increase was obtained from glyoxal than methylglyoxal, due to more complex interconversion between the latter and its products.

To verify the above hypothesis, the photolysis and photochemical oxidation of a mixture of glyoxal and methylglyoxal were further compared. At 10 min, the residual concentrations of glyoxal and methylglyoxal were 1885.4 ± 202.4 and 1108.3 ± 136.7 ppb in the photolysis system, and 1870.1 ± 181.8 and 1005.2 ± 73.1 ppb in the photochemical oxidation system. The higher consumption of methylglyoxal in both systems was due to its higher photolysis rate and ·OH reaction rate constant (Plum et al., 1983), and also because glyoxal was its product. When the reaction time was prolonged to 60 min, the concentration of methylglyoxal was virtually unchanged in the photolysis system (1102.6 ± 18.2 ppb), while it gradually decreased to 887.2 ± 77.0 ppb in the photochemical oxidation system. Glyoxal concentration showed identical variation trend of first decrease and then increase in both systems within 60 min, although higher consumption of glyoxal was observed in photochemical oxidation. Conversely, the concentration of formaldehyde increased from 102.5 ± 18.2 to 108.6 ± 10.4 ppb in the photochemical oxidation system, while decreased from 75.1 ± 2.1 to 55.8 ± 5.7 ppb in the photolysis system.

It was found that formaldehyde production was separately related to glyoxal photolysis and to photochemical oxidation of methylglyoxal (Fig. S26). In identical reaction systems, the concentration of formaldehyde from mixed glyoxal and methylglyoxal was higher than that from single methylglyoxal, but lower than that from single glyoxal, suggesting that methylglyoxal suppressed the transformation of glyoxal to formaldehyde. The enhanced consumption of methylglyoxal when mixed with glyoxal did not lead to remarkable production of either glyoxal or formaldehyde. However, the presence of glyoxal resulted in preferential conversion of methylglyoxal to other products such as hydrate. Theoretical and experimental studies have shown that liquid-phase methylglyoxal is hydrated to form methylglyoxal glycol (Krizner et al., 2009; Loeffler et al., 2006), while Jessica et al. also confirmed the formation of methylglyoxal glycol from methylglyoxal in gaseous phase (Axson et al., 2010), supporting the proposed hypothesis.

Photolysis of glyoxal and methylglyoxal mixture produced 5.4 ± 2.1 to 44.5 ± 3.7 μg m^{-3} of SOA (Fig. 4f), which was higher than that from photolysis of single glyoxal or methylglyoxal. Reaction of mixed dicarbonyl under light irradiation was conducive to the formation of SOA. Moreover, the produced SOA (10.6 ± 1.1 μg m^{-3}) from photochemical oxidation of mixed glyoxal and methylglyoxal for 10 min was about 21.2 or 8.2 times of that of single glyoxal or methylglyoxal. The significant consumption of methylglyoxal contributed to the enhanced formation of SOA. Although longer photochemical oxidation time led to higher SOA production (e.g., 27.7 ± 1.1 μg m^{-3} at 60 min), the current SOA mass concentration was still lower than that produced from photolysis of mixed glyoxal and methylglyoxal as well as from photochemical oxidation of single glyoxal or methylglyoxal. The reaction of methylglyoxal with ·OH preferentially produced other intermediates, which were reversibly converted to glyoxal and methylglyoxal, resulting in their accumulation. Thus, it was unfavorable for SOA formation.

3.5. Environmental implications

By calculating the mass-based ratio of the formed SOA and the reacted m-xylene at 120 min, SOA yield of 2.5% was obtained in this study. Under the same mass concentration of SOA (86.0 μg m^{-3}), about 14.3% of SOA yield was also calculated by theoretical simulation based on two-product semi-empirical model (Odum et al., 1996) and experimental fitting parameters of m-xylene from previous work (Li et al., 2016). The result obtained from theoretical prediction was over 5.7 times greater than that from experimental simulation, suggesting overestimation of theoretical modeling. Laboratory experiments and theoretical models have their own advantages in SOA investigation and many researchers have tried to revise the discrepancy between them (Ji et al., 2017; Vereecken and Francisco, 2012). The classical two-product semi-empirical model is based on the hypothesis that there are two kinds of semi-volatile products with low and high volatility. By comparison, monocarbonyl showed higher volatility than dicarbonyl when the number of carbon atoms was the same. Unfortunately, available works have focused on the importance of dicarbonyl in SOA formation, but ignored the contribution of monocarbonyl. The present results of photochemical oxidation of m-xylene confirmed that dicarbonyl was the dominant contributor for SOA formation, while monocarbonyl showed greater influence on the decreased SOA production. Therefore, during photochemical oxidation of m-xylene, one reason for the overestimation of SOA yield from theoretical calculation was ignoring the underappreciated role of monocarbonyl. The mutual transformation between dicarbonyl and monocarbonyl was also not taken into consideration. So far, only glyoxal, methylglyoxal and formaldehyde were chosen as representatives to reveal the role of their interconversion in the formation of SOA. However, there are many other important carbonyl-containing products, such as acetaldehyde, glycolaldehyde, pyruvic acid, dihydroxyacetone, etc., that are involved in SOA formation from oxidation of AHs (Shrivastava et al., 2017). More interconversions might happen among them to influence the SOA production. Therefore, comprehensive investigations are necessary to ascertain not only the interconversion but also the role of these active intermediates in SOA formation. Such data could efficiently establish the formation mechanism of SOA and complete the database of theoretical model to more accurately predict the SOA yield from AH oxidation in atmospheric environment.

CRediT authorship contribution statement

Jiangyao Chen: Methodology, Formal analysis, Writing – original draft, Conceptualization, Supervision. **Jiani Li:** Methodology, Formal analysis. **Xiaoyan Chen:** Methodology, Data curation. **Jianwei Gu:** Writing – review & editing. **Taicheng An:** Conceptualization.

Declaration of competing interest

The authors declare that they have no known competing financial interests or personal relationships that could have appeared to influence the work reported in this paper.

Acknowledgement

This work was financially supported by National Key R&D Program of China (2019YFC0214402), National Natural Science Foundation of China (42177354, 21777032), Local Innovative and Research Teams Project of Guangdong Pearl River Talents Program (2017BT01Z032), and Key-Area Research and Development Program of Guangdong Province (2019B110206002).

Appendix A. Supplementary data

The Supporting Information is available free of charge on the website. Additional information on experimental method and Figures of intermediate information. Supplementary data to this article can be found online at https://doi.org/10.1016/j.scitotenv.2021.152575.

References

Alvarez-Idaboy, J.R., Mora-Diez, N., Boyd, R.J., Vivier-Bunge, A., 2001. On the importance of prereactive complexes in molecule-radical reactions: hydrogen abstraction from aldehydes by OH. J. Am. Chem. Soc. 123 (9), 2018–2024.
Arey, J., Obermeyer, G., Aschmann, S.M., Chattopadhyay, S., Cusick, R.D., Atkinson, R., 2009. Dicarbonyl products of the OH radical-initiated reaction of a series of aromatic hydrocarbons. Environ. Sci. Technol. 43 (3), 683–689.
Atkinson, R., 1986. Kinetics and mechanisms of the gas-phase reactions of the hydroxyl radical with organic compounds under atmospheric conditions. Chem. Rev. 86 (1), 69–201.
Atkinson, R., Tuazon, E.C., Aschmann, S.M., 2000. Atmospheric chemistry of 2-pentanone and 2-heptanone. Environ. Sci. Technol. 34 (4), 623–631.
Axson, J.L., Takahashi, K., De Haan, D.O., Vaida, V., 2010. Gas-phase water-mediated equilibrium between methylglyoxal and its geminal diol. Proc. Natl. Acad. Sci. USA 107 (15), 6687–6692.
Birdsall, A.W., Elrod, M.J., 2011. Comprehensive NO-dependent study of the products of the oxidation of atmospherically relevant aromatic compounds. J. Phys. Chem. A 115 (21), 5397–5407.
Butkovskaya, N.I., Setser, D.W., 1998. Infrared chemiluminescence study of the reactions of hydroxyl radicals with formaldehyde and formyl radicals with H, OH, NO, and NO2. J. Phys. Chem. A 102 (48), 9715–9728.
Chen, Y.Q., Zhu, L., 2003. Wavelength-dependent photolysis of glyoxal in the 290–420 nm region. J. Phys. Chem. A 107 (23), 4643–4651.
Chen, Y.Q., Wang, W.J., Zhu, L., 2000. Wavelength-dependent photolysis of methylglyoxal in the 290–440 nm region. J. Phys. Chem. A 104 (47), 11126–11131.
Chen, J.Y., Yi, J.J., Ji, Y.M., Zhao, B.C., Ji, Y.P., Li, G.Y., An, T.C., 2020. Enhanced H-abstraction contribution for oxidation of xylenes via mineral particles: implications for particulate matter formation and human health. Environ. Res. 186, 109568.
Clifford, G.M., Hadj-Aissa, A., Healy, R.M., Mellouki, A., Munoz, A., Wirtz, K., Reviejo, M.M., Borras, E., Wenger, J.C., 2011. The atmospheric photolysis of o-tolualdehyde. Environ. Sci. Technol. 45 (22), 9649–9657.
Duarte, R.M.B.O., Pio, C.A., Duarte, A.C., 2005. Spectroscopic study of the water-soluble organic matter isolated from atmospheric aerosols collected under different atmospheric conditions. Anal. Chim. Acta 530 (1), 7–14.
Edney, E.O., Kleindienst, T.E., Jaoui, M., Lewandowski, M., Offenberg, J.H., Wang, W., Claeys, M., 2005. Formation of 2-methyl tetrols and 2-methylglyceric acid in secondary organic aerosol from laboratory irradiated isoprene/NOX/SO2/air mixtures and their detection in ambient PM2.5 samples collected in the eastern United States. Atmos. Environ. 39 (29), 5281–5289.
Fan, J.W., Zhang, R.Y., 2008. Density functional theory study on OH-initiated atmospheric oxidation of m-xylene. J. Phys. Chem. A 112 (18), 4314–4323.
Feierabend, K.J., Zhu, L., Talukdar, R.K., Burkholder, J.B., 2008. Rate coefficients for the OH + HC(O)C(O)H (glyoxal) reaction between 210 and 390. J. Phys. Chem. A 112 (1), 73–82.
Fu, T.M., Jacob, D.J., Wittrock, F., Burrows, J.P., Vrekoussis, M., Henze, D.K., 2008. Global budgets of atmospheric glyoxal and methylglyoxal, and implications for formation of secondary organic aerosols. J. Geophys. Res.-Atmos. 113 (D15).
Gomez Alvarez, E., Viidanoja, J., Munoz, A., Wirtz, K., Hjorth, J., 2007. Experimental confirmation of the dicarbonyl route in the photo-oxidation of toluene and benzene. Environ. Sci. Technol. 41 (24), 8362–8369.
Hallquist, M., Wenger, J.C., Baltensperger, U., Rudich, Y., Simpson, D., Claeys, M., Dommen, J., Donahue, N.M., George, C., Goldstein, A.H., Hamilton, J.F., Herrmann, H., Hoffmann, T., Iinuma, Y., Jang, M., Jenkin, M.E., Jimenez, J.L., Kiendler-Scharr, A., Maenhaut, W., McFiggans, G., Mentel, T.F., Monod, A., Prevot, A.S.H., Seinfeld, J.H., Surratt, J.D., Szmigielski, R., Wildt, J., 2009. The formation, properties and impact of secondary organic aerosol: current and emerging issues. Atmos. Chem. Phys. 9 (14), 5155–5236.
Henze, D.K., Seinfeld, J.H., Ng, N.L., Kroll, J.H., Fu, T.M., Jacob, D.J., Heald, C.L., 2008. Global modeling of secondary organic aerosol formation from aromatic hydrocarbons: high- vs. low-yield pathways. Atmos.Chem. Phys. 8 (9), 2405–2420.
Hepburn, J.W., Buss, R.J., Butler, L.J., Lee, Y.T., 1983. Molecular beam study of the photochemistry of S1 glyoxal. J. Phys. Chem. 87, 3638–3641.
Herckes, P., Valsaraj, K.T., Collett, J.L., 2013. A review of observations of organic matter in fogs and clouds: origin, processing and fate. Atmos. Res. 132, 434–449.

Hu, W.W., Campuzano-Jost, P., Palm, B.B., Day, D.A., Ortega, A.M., Hayes, P.L., Krechmer, J.E., Chen, Q., Kuwata, M., Liu, Y.J., de Sa, S.S., McKinney, K., Martin, S.T., Hu, M., Budisulistiorini, S.H., Riva, M., Surratt, J.D., St Clair, J.M., Isaacman-Van Wertz, G., Yee, L.D., Goldstein, A.H., Carbone, S., Brito, J., Artaxo, P., de Gouw, J.A., Koss, A., Wisthaler, A., Mikoviny, T., Karl, T., Kaser, L., Jud, W., Hansel, A., Docherty, K.S., Alexander, M.L., Robinson, N.H., Coe, H., Allan, J.D., Canagaratna, M.R., Paulot, F., Jimenez, J.L., 2015. Characterization of a real-time tracer for isoprene epoxydiols-derived secondary organic aerosol (IEPOX-SOA) from aerosol mass spectrometer measurements. Atmos. Chem. Phys. 15 (20), 11807–11833.

Huang, D., Chen, Z.M., Zhao, Y., Liang, H., 2013. Newly observed peroxides and the water effect on the formation and removal of hydroxyalkyl hydroperoxides in the ozonolysis of isoprene. Atmos. Chem. Phys. 13 (11), 5671–5683.

Ji, Y.M., Zhao, J., Terazono, H., Misawa, K., Levitt, N.P., Li, Y.X., Lin, Y., Peng, J.F., Wang, Y., Duan, L., Pan, B.W., Zhang, F., Feng, X.D., An, T.C., Marrero-Ortiz, W., Secrest, J., Zhang, A.L., Shibuya, K., Molina, M.J., Zhang, R.Y., 2017. Reassessing the atmospheric oxidation mechanism of toluene. Proc. Natl. Acad. Sci. USA 114 (31), 8169–8174.

Ji, Y.M., Shi, Q.J., Li, Y.X., An, T.C., Zheng, J., Peng, J.F., Gao, Y.P., Chen, J.Y., Li, G.Y., Wang, Y., Zhang, F., Zhang, A.L., Zhao, J.Y., Molina, M.J., Zhang, R.Y., 2020. Carbenium ion-mediated oligomerization of methylglyoxal for secondary organic aerosol formation. Proc. Natl. Acad. Sci. USA 117 (24), 13294–13299.

Koziel, J.A., Noah, J., Pawliszyn, J., 2001. Field sampling and determination of formaldehyde in indoor air with solid-phase microextraction and on-fiber derivatization. Environ. Sci. Technol. 35 (7), 1481–1486.

Krizner, H.E., De Haan, D.O., Kua, J., 2009. Thermodynamics and kinetics of methylglyoxal dimer formation: a computational study. J. Phys. Chem. A 113 (25), 6994–7001.

Kroll, J.H., Ng, N.L., Murphy, S.M., Flagan, R.C., Seinfeld, J.H., 2006. Secondary organic aerosol formation from isoprene photooxidation. Environ. Sci. Technol. 40 (6), 1869–1877.

Kua, J., Krizner, H.E., De Haan, D.O., 2011. Thermodynamics and kinetics of imidazole formation from glyoxal and methylamine: a computational study. J. Phys. Chem. A 115, 1667–1675.

Li, Z., Schwier, A.N., Sareen, N., McNeill, V.F., 2011. Reactive processing of formaldehyde and acetaldehyde in aqueous aerosol mimics: surface tension depression and secondary organic products. Atmos. Chem. Phys. 11, 11617–11629.

Li, L., Tang, P., Nakao, S., Chen, C.L., Cocker, D.R., 2016. Role of methyl group number on SOA formation from monocyclic aromatic hydrocarbons photooxidation under low-NOx conditions. Atmos. Chem. Phys. 16 (4), 2255–2272.

Li, L.J., Qi, L., Cocker, D.R., 2017. Contribution of methyl group to secondary organic aerosol formation from aromatic hydrocarbon photooxidation. Atmos. Environ. 151, 133–139.

Li, J., Chen, J.Y., Ji, Y.M., Wang, J.X., Li, G.Y., An, T.C., 2019. Solar light induced transformation mechanism of allyl alcohol to monocarbonyl and dicarbonyl compounds on different TiO2: a combined experimental and theoretical investigation. Chemosphere 232, 287–295.

Li, Q.Q., Su, G.J., Li, C.Q., Liu, P.F., Zhao, X.X., Zhang, C.L., Sun, X., Mu, Y.J., Wu, M.G., Wang, Q.L., Sun, B.H., 2020. An investigation into the role of VOCs in SOA and ozone production in Beijing,China. Sci. Total Environ. 720, 137536.

Loeffler, K.W., Koehler, C.A., Paul, N.M., De Haan, D.O., 2006. Oligomer formation in evaporating aqueous glyoxal and methyl glyoxal solutions. Environ. Sci. Technol. 40 (20), 6318–6323.

Luo, H., Chen, J.Y., Li, G.Y., An, T.C., 2021. Formation kinetics and mechanisms of ozone and secondary organic aerosols from photochemical oxidation of different aromatic hydrocarbons: dependence on NOx and organic substituents. Atmos. Chem. Phys. 21 (10), 7567–7578.

Marais, E.A., Jacob, D.J., Jimenez, J.L., Campuzano-Jost, P., Day, D.A., Hu, W., Krechmer, J., Zhu, L., Kim, P.S., Miller, C.C., Fisher, J.A., Travis, K., Yu, K., Hanisco, T.F., Wolfe, G.M., Arkinson, H.L., Pye, H.O.T., Froyd, K.D., Liao, J., McNeill, V.F., 2016. Aqueous-phase mechanism for secondary organic aerosol formation from isoprene: application to the southeast United States and co-benefit of SO2 emission controls. Atmos. Chem. Phys. 16 (3), 1603–1618.

Ng, N.L., Kroll, J.H., Chan, A.W.H., Chhabra, P.S., Flagan, R.C., Seinfeld, J.H., 2007. Secondary organic aerosol formation from m-xylene, toluene, and benzene. Atmos. Chem. Phys. 7 (14), 3909–3922.

Nishino, N., Arey, J., Atkinson, R., 2010. Formation yields of glyoxal and methylglyoxal from the gas-phase OH radical-initiated reactions of toluene, xylenes, and trimethylbenzenes as a function of NO2 concentration. J. Phys. Chem. A 114 (37), 10140–10147.

Odum, J.R., Hoffmann, T., Bowman, F., Collins, D., Flagan, R.C., Seinfeld, J.H., 1996. Gas/particle partitioning and secondary organic aerosol yields. Environ. Sci. Technol. 30, 2580–2585.

Pan, S.S., Wang, L.M., 2014. Atmospheric oxidation mechanism of m-xylene initiated by OH radical. J. Phys. Chem. A 118 (45), 10778–10787.

Pang, X., Lewis, A.C., Rickard, A.R., Baeza-Romero, M.T., Adams, T.J., Ball, S.M., Daniels, M.J.S., Goodall, I.C.A., Monks, P.S., Peppe, S., Garcia, M.R., Sanchez, P., Munoz, A., 2014. A smog chamber comparison of a microfluidic derivatisation measurement of gas-phase glyoxal and methylglyoxal with other analytical techniques. Atmos. Meas. Tech. 7 (2), 373–389.

Paulot, F., Crounse, J.D., Kjaergaard, H.G., Kurten, A., St Clair, J.M., Seinfeld, J.H., Wennberg, P.O., 2009. Unexpected epoxide formation in the gas-phase photooxidation of isoprene. Science 325 (5941), 730–733.

Perri, M.J., Seitzinger, S., Turpin, B.J., 2009. Secondary organic aerosol production from aqueous photooxidation of glycolaldehyde: laboratory experiments. Atmos. Environ. 43 (8), 1487–1497.

Plum, C.N., Sanhueza, E., Atkinson, R., Carter, W.P.L., Pitts, J.N., 1983. OH radical rate constants and photolysis rates of a-dicarbonyls. Environ. Sci. Technol. 17, 479–484.

Riva, M., Robinson, E.S., Perraudin, E., Donahue, N.M., Villenave, E., 2015. Photochemical aging of secondary organic aerosols generated from the photooxidation of polycyclic aromatic hydrocarbons in the gas-phase. Environ. Sci. Technol. 49 (9), 5407–5416.

Rodriguez, A.A., de Loera, A., Powelson, M.H., Galloway, M.M., Haan, D.O., 2017. Formaldehyde and acetaldehyde increase aqueous-phase production of imidazoles in methylglyoxal/amine mixtures: quantifying a secondary organic aerosol formation mechanism. Environ. Sci. Technol. Lett. 4 (6), 234–239.

Santos, E.B.H., Duarte, A.C., 1998. The influence of pulp and paper mill effluents on the composition of the humic fraction of aquatic organic matter. Water Res. 32 (3), 597–608.

Sato, K., Takami, A., Isozaki, T., Hikida, T., Shimono, A., Imamura, T., 2010. Mass spectrometric study of secondary organic aerosol formed from the photo-oxidation of aromatic hydrocarbons. Atmos. Environ. 44 (8), 1080–1087.

Sedehi, N., Takano, H., Blasic, V.A., Sullivan, K.A., De Haan, D.O., 2013. Temperature- and pH-dependent aqueous-phase kinetics of the reactions of glyoxal and methylglyoxal with atmospheric amines and ammonium sulfate. Atmos. Environ. 77, 656–663.

Shrivastava, M., Cappa, C.D., Fan, J.W., Goldstein, A.H., Guenther, A.B., Jimenez, J.L., Kuang, C., Laskin, A., Martin, S.T., Ng, N.L., Petaja, T., Pierce, J.R., Rasch, P.J., Roldin, P., Seinfeld, J.H., Shilling, J., Smith, J.N., Thornton, J.A., Volkamer, R., Wang, J., Worsnop, D.R., Zaveri, R.A., Zelenyuk, A., Zhang, Q., 2017. Recent advances in understanding secondary organic aerosol: implications for global climate forcing. Rev. Geophys. 55 (2), 509–559.

Smith, D.F., Kleindienst, T.E., McIver, C.D., 1999. Primary product distributions from the reaction of OH with m-, p-xylene, 1,2,4- and 1,3,5-trimethylbenzene. J. Atmos. Chem. 34 (3), 339–364.

Song, M., Zhang, C.L., Wu, H., Mu, Y.J., Ma, Z.B., Zhang, Y.Y., Liu, J.F., Li, X.R., 2019. The influence of OH concentration on SOA formation from isoprene photooxidation. Sci. Total Environ. 650, 951–957.

Stief, L.J., Nava, D.F., Payne, W.A., Michael, J.V., 1980. Rate constant for the reaction of hydroxyl radical with formaldehyde over the temperature range 228–362 K. J. Chem. Phys. 73, 2254–2258.

Tadic, J., Moortgat, G.K., Wirtz, K., 2006. Photolysis of glyoxal in air. J. Photochem. Photobiol. A 177 (2–3), 116–124.

Teng, A.P., Crounse, J.D., Wennberg, P.O., 2017. Isoprene peroxy radical dynamics. J. Am. Chem. Soc. 139 (15), 5367–5377.

Tuazon, E.C., Atkinson, R., Aschmann, S.M., Arey, J., Winer, A.M., Pittts, J.N., 1986. Atmospheric loss processes of 1,2-dibromo-3-chloropropane and trimethyl phosphate. Environ. Sci. Technol. 20 (10), 1043–1046.

Vereecken, L., Francisco, J.S., 2012. Theoretical studies of atmospheric reaction mechanisms in the troposphere. Chem. Soc. Rev. 41 (19), 6259–6293.

Volkamer, R., Platt, U., Wirtz, K., 2001. Primary and secondary glyoxal formation from aromatics: experimental evidence for the bicycloalkyl-radical pathway from benzene, toluene, and p-xylene. J. Phys. Chem. A 105 (33), 7865–7874.

Wang, S.Y., Wu, D.W., Wang, X.M., Fung, J.C.H., Yu, J.Z., 2013. Relative contributions of secondary organic aerosol formation from toluene, xylenes, isoprene, and monoterpenes in Hong Kong and Guangzhou in the Pearl River Delta, China: an emission-based box modeling study. J. Geophys. Res.-Atmos. 118 (2), 507–519.

Ying, Q., Li, J.Y., Kota, S.H., 2015. Significant contributions of isoprene to summertime secondary organic aerosol in Eastern United States. Environ. Sci. Technol. 49 (13), 7834–7842.

Yu, J.Z., Jeffries, H.E., Le Lacheur, R.M., 1995. Identifying airborne carbonyl compounds in isoprene atmospheric photooxidation products by their PFBHA oximes using gas chromatography/ion trap mass spectrometry. Environ. Sci. Technol. 29 (8), 1923–1932.

Zhang, H., Surratt, J.D., Lin, Y.H., Bapat, J., Kamens, R.M., 2011. Effect of relative humidity on SOA formation from isoprene/NO photooxidation: enhancement of 2-methylglyceric acid and its corresponding oligoesters under dry conditions. Atmos. Chem. Phys. 11 (13), 6411–6424.

Zhang, Q., Xu, Y.F., Jia, L., 2019. Secondary organic aerosol formation from OH-initiated oxidation of m-xylene: effects of relative humidity on yield and chemical composition. Atmos. Chem. Phys. 19 (23), 15007–15021.

Zhang, P., Huang, J.Y., Shu, J.N., Yang, B., 2019. Comparison of secondary organic aerosol (SOA) formation during o-, m-, and p-xylene photooxidation. Environ. Pollut. 245, 20–28.